

236 μ W Direct-RF PLL-Free Multi-PSK Transmitter Using Oscillator-Based Phase Synthesis

Meysam Sohani Darban¹, Fariborz Lohrabi Pour², Dong Sam Ha¹, Jeffrey Sean Walling¹

¹Virginia Polytechnic Institute and State University, Blacksburg, VA, USA

²University of North Carolina at Charlotte, Charlotte, NC, USA

Emails: meysam97@vt.edu, flohrabi@charlotte.edu, ha@vt.edu, jswalling@vt.edu

Abstract—This paper presents a compact, low-power, direct RF multi-phase-shift keying (PSK) transmitter (TX) that eliminates the need for a phase-locked loop (PLL) by performing phase modulation directly within a ring oscillator. The proposed architecture exploits synchronized charge extraction at the oscillator’s transition points to induce controlled phase shifts while maintaining constant amplitude and frequency. A time-domain multi-triggering technique is introduced to enable reconfigurable multi-mode modulation, supporting 16-PSK, 8-PSK, QPSK, and BPSK within a unified hardware structure. The TX circuit is fabricated in a 22-nm FD-SOI process and operates in the ISM band at 2.4 GHz. Measurement results indicate a symbol rate of 2 MSps with a maximum error vector magnitude (EVM) of 5.13% rms. The core TX occupies $23 \times 17.6 \mu\text{m}^2$ and consumes 236 μ W, excluding the output driver, which delivers -10 dBm output power over a 60 MHz bandwidth. The proposed design achieves a favorable trade-off between power consumption, circuit complexity, and modulation flexibility, making it well-suited for low-power wireless applications.

Index Terms—Direct RF modulation, low-power, phase-shift keying (PSK), time-domain phase synthesis, transmitter (TX).

I. INTRODUCTION

The rapid proliferation of ultra-low-power wireless systems for Internet-of-Things (IoT), biomedical, and distributed sensing has exposed fundamental limitations in conventional RF transmitter (TX) architectures [1], [2]. Although phase-locked loop (PLL)-based TXs dominate in modern systems, their power consumption, complexity, and die area make them prohibitive for energy-constrained platforms operating at sub-milliwatt power levels while maintaining acceptable modulation accuracy [3], [4]. This underscores the need for alternative architectures that bypass the overhead of frequency synthesis while still supporting robust and reliable modulation.

Phase-shift keying (PSK) remains a preferred modulation scheme for low-power systems due to its resilience to amplitude noise and channel fading [5]. However, most existing PSK TXs rely on PLLs or discrete phase-synthesis techniques (e.g., controlled delay elements), leading to phase mismatch, linearity degradation, calibration overhead, and large area consumption [3], [6], while failing to exploit the oscillator’s intrinsic phase dynamics, and thereby limiting their efficiency in low-power operation.

This work demonstrates that scalable PSK can be achieved directly via oscillator phase dynamics, without reliance on a PLL or a phase-interpolation network. Despite prior oscillator-based approaches that suffered from limited controllability or

coarse phase resolution, the proposed architecture introduces a deterministic phase manipulation based on synchronized charge extraction at the oscillator’s maximum phase-sensitivity points [7]. Leveraging the oscillator’s natural charge-to-phase translation mechanism, repeatable phase shifts are achieved while maintaining constant amplitude and frequency.

A key innovation of this work is the introduction of a multi-triggering modulation strategy that redefines how phase resolution is achieved in RF TXs. The proposed technique encodes baseband information by accumulating discrete phase adjustments of a constant value in the time domain, rather than using analog tuning elements (e.g., large capacitor banks [8]), thereby enabling multi-level PSK with a single compact hardware structure. This removes the trade-off between phase resolution and complexity, while supporting reconfigurable modulation without additional hardware overhead. The resulting architecture represents a transition toward digitally assisted, oscillator-centric RF TXs, where phase modulation is employed directly in the signal generation process.

This article is organized as follows. Section II presents the theoretical foundation of oscillator-based phase modulation and describes the proposed multi-PSK TX architecture and performance considerations. Section III describes the measurement results, and finally, Section IV concludes the paper.

II. DIRECT RF MULTI-PSK TRANSMITTER

This section explains the concept of the oscillator-based PSK modulation, providing a description of the proposed TX architecture with analysis of its performance considerations.

A. Oscillator-Based Phase Shift Keying Concepts

In a PSK TX, the carrier’s phase varies while its amplitude remains constant. The oscillator can perform this function via direct modulation, but in most cases, it is done in the baseband. In the case of direct modulation, one way to characterize the oscillator’s performance is to view it as charging and discharging its output nodes within each operating period while maintaining stable oscillation. If any additional charge is injected or drawn from these output nodes, it can perturb both the amplitude and phase of the signal. Fig. 1 illustrates the effect of injecting the charge Δq_{inj} into the output capacitor of the oscillator (C_{out}) at two critical time instances. The red line shows the signal deviation when injecting at the zero-crossing point, while the blue line is the response of the oscillator to

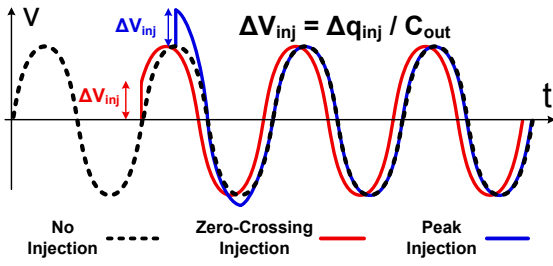


Fig. 1. Charge injection effect at different moments of an oscillator's output.

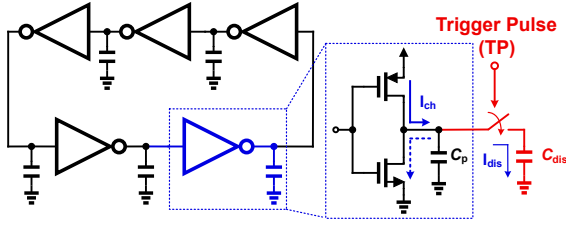


Fig. 2. Concept of charge extraction on a ring oscillator.

the charge injection at the peak amplitude. This extra charge causes a voltage change across the output capacitor equal to:

$$\Delta V_{inj} = \frac{\Delta q_{inj}}{C_{out}}. \quad (1)$$

Owing to the self-limiting nature of the oscillator and the constraints of the power supply, any variations in amplitude are suppressed, which ensures that the output remains constant [9]. Alternatively, the effect of the excess charge on the phase of the voltage waveform remains. This phase variation depends on the injection time. As discussed in [7], the impulse sensitivity function (ISF) of an oscillator relates this dependency. For a ring oscillator, if the excess charge is injected at the signal's amplitude peaks, there will be no phase shift in the waveform. Conversely, the maximum phase shift occurs when the charge is injected at the zero-crossing points.

The ring oscillator shown in Fig. 2 consists of an odd number of inverters with a charging current of I_{ch} followed by a total output capacitor (parasitic and fixed) of C_p . While oscillating, the oscillator charges/discharges C_p during each cycle. The output current of each stage and the amount of charge that sinks or sources each node's equivalent capacitor determine the circuit's frequency. If the capacitor C_{dis} , with no initial charge, is momentarily connected to an oscillator output node via an ideal switch controlled by a trigger pulse (TP), a portion of I_{ch} flows into C_{dis} as a discharge current (I_{dis}). This process extracts the charge that would otherwise contribute to C_p . If the switch turns on for a short period, this acts as the charge injection described in Fig. 1.

The TP's timing relative to the output signal defines the window at which charge extraction occurs. Two main factors that determine the extent of phase adjustment achievable at the output are the timing of the TP, due to the ISF, and the ratio of C_{dis} to C_p , which dictates the amount of charge that can be drawn from the output node. For a ring oscillator, the ISF peaks at the transition points from 0 to V_{DD} [9]. By

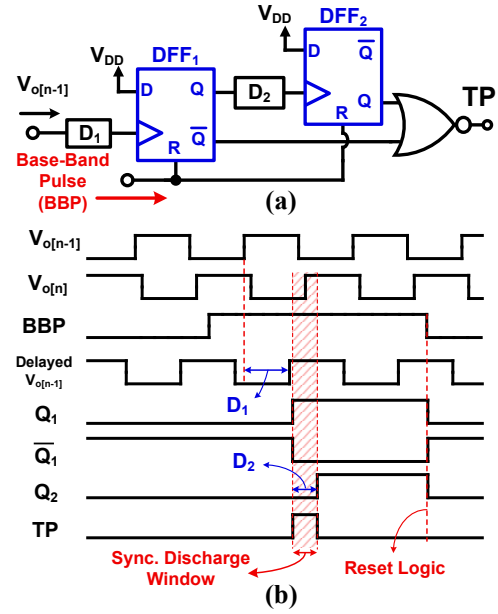


Fig. 3. (a) Schematic of proposed control unit circuit, and (b) logic wave forms corresponding to creating a TP window.

ensuring that the TP's timing is synchronized to this transition point and using a properly sized capacitor at one node of the ring oscillator, the circuit develops controllable phase shifts while maintaining constant frequency and amplitude, which is essential for a PSK TX. Controlling the capacitor and the TP's timing leads to a direct RF-oscillator-based PSK modulator.

B. Transmitter Circuit Design

To provide a timing window for TP, a digital control unit has been designed that generates a window, synchronized to the rising edge of the oscillator's output, for each baseband pulse (BBP) received from the baseband modem. Fig. 3 (a) displays the proposed circuit. The control unit will utilize the output of one stage of oscillator, $V_{o[n-1]}$, and generate a narrow timing window over the rising edge of the next stage's output, $V_{o[n]}$.

As illustrated in Fig. 3 (b), when BBP is set to 0, the DFFs are in the reset state. When BBP is 1, the first DFF can function on the rising edge of its clock, provided by the D_1 delay path. Then, by sensing the rising edge, the $Q_1(\bar{Q}_1)$ will be set to 1(0). Changing the \bar{Q}_1 will raise the TP to 1, which is the TP window's first edge. After the rising edge of Q_1 passes through the D_2 's delay line, it changes the second DFF's outputs. As a result, TP returns to 0 again, creating the second edge of the TP window. Lastly, when the BBP returns to 0, the control unit's signals will be reset and ready for the next data transmission cycle. As shown in Fig. 3 (b), D_1 determines the position of the window, and D_2 defines its width. D_1 and D_2 were optimized to keep the rising edge within the window across all PVT variations so the charge extraction can trigger the ISF most effectively.

The schematic of the proposed PSK TX is illustrated in Fig. 4. When the TP window turns on the M_1 switch, it connects the C_{dis} to the $V_{o[n]}$ and draws a portion of its charge while it tries to raise $V_{o[n]}$ to V_{DD} , leading to a

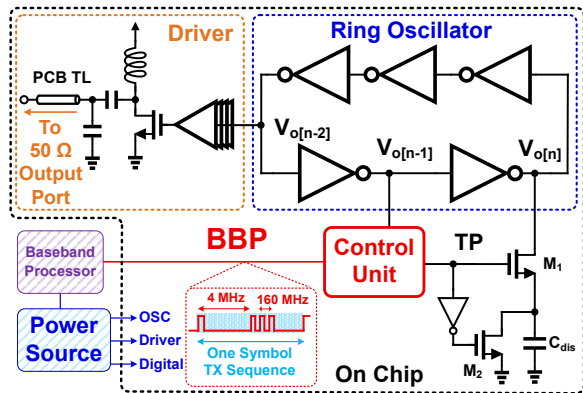


Fig. 4. Schematic of proposed direct RF PSK TX.

constant phase shift over the operation phase of the oscillator. In addition, in reset mode, the M_2 ensures the C_{dis} is in a zero-charge state before connection. The other output of the oscillator is connected to a buffer chain, which drives a power driver transistor, sending the RF data to the output pad via a matching network and the PCB transmission line (TL). A microcontroller can handle the baseband processing and generate the required BBP sequences for the TX to send data.

C. Performance Considerations

The phase shift of this circuit is constant; however, PSK requires different phases for the RF carrier. One approach is to change the phase using a bank of capacitors. However, simulation results indicate linearity degradation across different symbols due to non-idealities in the capacitor bank and its switch behavior. Additionally, the capacitor bank increases the die area, which is not fit for a compact all-digital design.

To address this issue, a multi-triggering technique is proposed. As the width of the TP window and the value of C_{dis} are set to provide only 22.5° of phase adjustment each time the TP window is applied. This phase adjustment is considered the phase-shift least significant bit (LSB) of the TX's modulation, thereby enabling standard 16PSK. Since all required phases of the target modulation are integer multiples of the circuit's LSB, to transmit each symbol from this modulation, the baseband must apply an integer number of BBPs in one baseband clock period. The multi-triggering technique and the proposed ring oscillator-based PSK result in a simple, compact PSK TX.

One advantage of the multi-triggering strategy is that the TX can dynamically define its effective LSB based on the number of generated triggers. For instance, if the processor generates two BBPs per circuit LSB, the TX effectively operates as an 8PSK modulator. Consequently, the proposed circuit can support multiple PSK modulation modes.

A limitation of the multi-triggering strategy is its inherent hysteresis, which can be solved by employing differential phase-shift keying (DPSK) instead of conventional PSK. In this method, the TX initially sends a reference symbol using a single BBP to establish a phase reference at the receiver. Subsequent symbols are generated using a variable number of BBPs, 1-16, to convey the desired data as illustrated in Fig. 4.

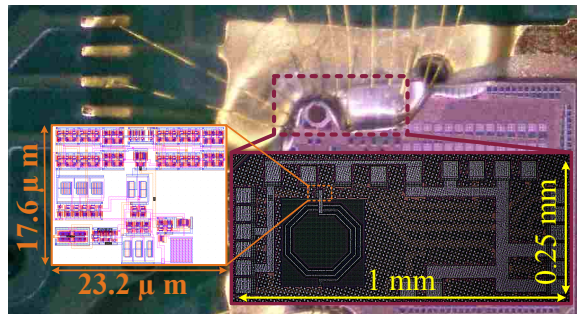


Fig. 5. Chip photograph and the layout of the proposed TX.

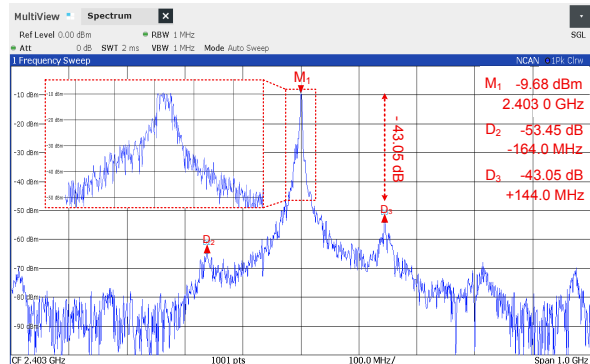


Fig. 6. Measured output spectrum.

The absence of a continuous reference frequency is architecturally justified by the well-established philosophy of asymmetric complexity, which shifts the synchronization burden to the receiver and prioritizes extreme energy efficiency and a minimal die area for the TX. With direct time-domain phase modulation of the oscillator via synchronous charge extracting, this design avoids the power-hungry frequency synthesis normally required in RF transmission. Although the lack of a feedback mechanism might lead to frequency drift, the design automatically compensates for this issue because DPSK is used as the modulation method. This allows the receiver equipped with Clock and Data Recovery (CDR) to effectively phase-lock onto the carrier and sync with the bit stream, thereby moving the burden of frequency stabilization from the power-limited TX to the power-rich receiver. Moreover, if higher-frequency accuracy is needed, a low-duty-cycle PLL may be added on the TX side for occasional calibration. Such a burst-mode calibration technique will enable correcting long-term frequency centering without the overhead associated with a fully functional frequency synthesizer.

III. MEASUREMENT RESULTS

The proposed 2.4 GHz multi-PSK TX was fabricated using 22-nm FD-SOI process technology. The die photo and the core digital TX's layout are shown in Fig. 5. The total occupied area (including pads) is $1 \times 0.25 \text{ mm}^2$, whereas the all digital core TX, excluding the driver, only occupied $23.2 \times 17.6 \text{ } \mu\text{m}^2$. The TX's maximum symbol rate is set at 2 MSps due to two primary constraints: the time required for the oscillator to settle into an adjusted phase and the digital processing unit's

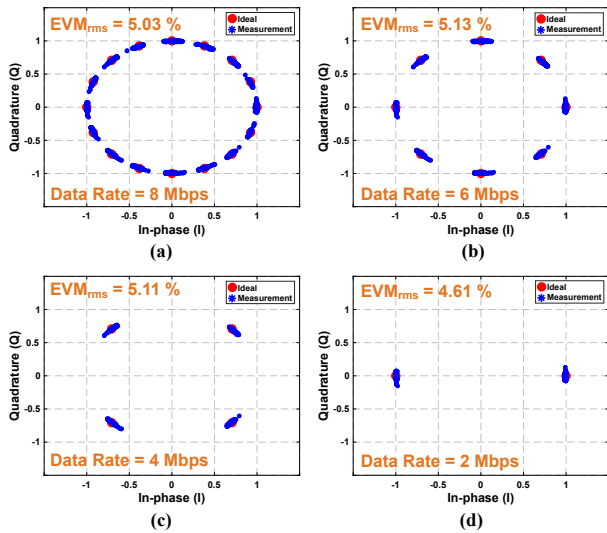


Fig. 7. TX's constellations for (a) 16DPSK, (b) 8DPSK, (c) QDPSK, and (d) BDPSK at 2 MSps.

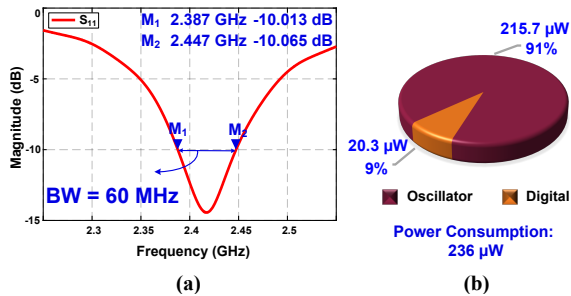


Fig. 8. (a) Measured output matching performance, and (b) power breakdown.

speed limits in generating TP windows. To achieve this rate using DPSK, the design employs a 4 MHz baseband clock for symbols and a 160 MHz BBP window rate.

Fig. 6 shows the output spectrum of the TX with baseband intermodulations on both sides of the main carrier, each at least 43 dB lower than the carrier tone. Fig. 7 illustrates the measured PSK constellations. Fig. 7 (a) illustrates the constellation for 16DPSK vs ideal symbols over 2 MHz, which is equal to 8 Mbps. Based on the measurement results, the root-mean-square (RMS) error vector magnitude (EVM) of the circuit is 5.03%, which is due to the oscillator phase noise. Since the circuit can operate in multi-DPSK modes, its performance at the same symbol rate in 8DPSK, QDPSK, and BDPSK is shown in Figs. 7 (b)–(d), respectively.

The on-chip matching network, including the PCB interconnection, is measured (S_{11}) and shown in Fig. 8 (a), which maintains $S_{11} < -10$ dB over a 60 MHz bandwidth centered at 2.4 GHz for the TX. The TX's power breakdown is displayed in Fig. 8 (b) using measured power and simulation results. The total power consumption, excluding the driver, is 236 μ W. While the output driver's power dissipation is 4.3 mW to deliver -10 dBm output power. Table I summarizes the design's performance compared to state-of-the-art works, indicating better energy-per-bit efficiency and significantly lower power consumption and core area due to the PLL-free design.

TABLE I
MEASURED PERFORMANCE SUMMARY AND COMPARISON

	This Work	[3]	[6]	[4]	[2]
Technology	22 nm FD-SOI	22 nm FD-SOI	65 nm	22 nm FD-SOI	65 nm
Standard / Modulation	ISM band/ (16, 8, Q, B) DPSK	BT, BLE, 802.15.4 / 8PSK	ISM Band / 8PSK	BLE / GFSK	BLE / GFSK
Architecture	Direct RF TX	PLL-TX	Injection Lock PA	PLL-TX	Polar-TX
Data rate (Mbps)	8 / 6 / 4 / 2	0.125 - 3	15	1 / 2	1
EVM_{rms} (%)	4.61 - 5.13	6.07	3.43 / 2.05	-	-
Energy/bit (nJ/bit)	0.0295 ***	0.83	0.57 / 0.48	1.32 / 0.66	1.2
P_{DC}^* (mW)	0.236	2.49 / 2.97	8.48 / 7.2	1.32	1.2
Core Area** (mm ²)	408 μ m ²	0.35	0.26	0.9	0.4

* Excluding driver (PA). ** Estimated TX area. *** 16-DPSK at 8 Mbps.

IV. CONCLUSION

This paper presents a low-power, multi-PSK ring-oscillator-based TX fabricated in 22-nm FD-SOI technology for the 2.4 GHz ISM band. The architecture eliminates the conventional PLL by performing phase modulation directly within the oscillator via synchronized charge extraction. By employing a time-domain multi-triggering technique, the design supports reconfigurable 16DPSK, 8DPSK, QDPSK, and DBPSK modulation schemes. Measurement results demonstrate a maximum EVM of 5.13% at 2 MSps. Excluding the driver, the core transmitter occupies a compact area of $23.2 \times 17.6 \mu$ m² and consumes only 236 μ W. These results validate the proposed design as a highly energy-efficient and scalable solution for ultra-low-power wireless IoT and biomedical applications.

V. ACKNOWLEDGMENT

The authors would like to acknowledge GlobalFoundries' University Partner Program for their chip fabrication support.

REFERENCES

- [1] H. Huang *et al.*, "Design of a compact low-power sub-2.4-GHz transceiver for medical band applications," *IEEE Journal of Solid-State Circuits*, vol. 60, no. 5, pp. 1516–1528, 2025.
- [2] H. Liu *et al.*, "An ADPLL-centric bluetooth low-energy transceiver with 2.3mW interference-tolerant hybrid-loop receiver and 2.9mW single-point polar transmitter in 65nm CMOS," in *2018 IEEE International Solid-State Circuits Conference - (ISSCC)*, 2018, pp. 444–446.
- [3] N. Scolari *et al.*, "23.2 a 1mm² software-defined dual-mode bluetooth transceiver with 10dBm maximum TX power and -98.2dBm sensitivity 2.96mW rx power at 1Mb/s," in *2024 IEEE International Solid-State Circuits Conference (ISSCC)*, vol. 67, 2024, pp. 402–404.
- [4] M. Tamura *et al.*, "30.5 a 0.5v BLE transceiver with a 1.9mW RX achieving -96.4dBm sensitivity and 4.1dB adjacent channel rejection at 1MHz offset in 22nm FDSOI," in *2020 IEEE International Solid-State Circuits Conference - (ISSCC)*, 2020, pp. 468–470.
- [5] J. Qian, A. N. Parks, J. R. Smith, F. Gao, and S. Jin, "IoT communications with M-psk modulated ambient backscatter: Algorithm, analysis, and implementation," *IEEE Internet of Things Journal*, vol. 6, no. 1, pp. 844–855, 2019.
- [6] S. Zargham, A. Datta, and A. Liscidini, "A 2.4-GHz 1.2-dBm 8PSK TX based on a class-C injection-locked power amplifier," in *2024 IEEE European Solid-State Electronics Research Conference (ESSERC)*, 2024, pp. 101–104.
- [7] A. Hajimiri and T. Lee, "A general theory of phase noise in electrical oscillators," *IEEE Journal of Solid-State Circuits*, vol. 33, no. 2, pp. 179–194, 1998.
- [8] F. L. Pour and D. S. Ha, "An M-PSK modulated polar transmitter based on a ring oscillator with low power and low design complexity for IoT applications," in *2022 IEEE International Symposium on Circuits and Systems (ISCAS)*, 2022, pp. 2182–2186.
- [9] A. Hajimiri, S. Limotyrakis, and T. Lee, "Jitter and phase noise in ring oscillators," *IEEE Journal of Solid-State Circuits*, vol. 34, no. 6, pp. 790–804, 1999.